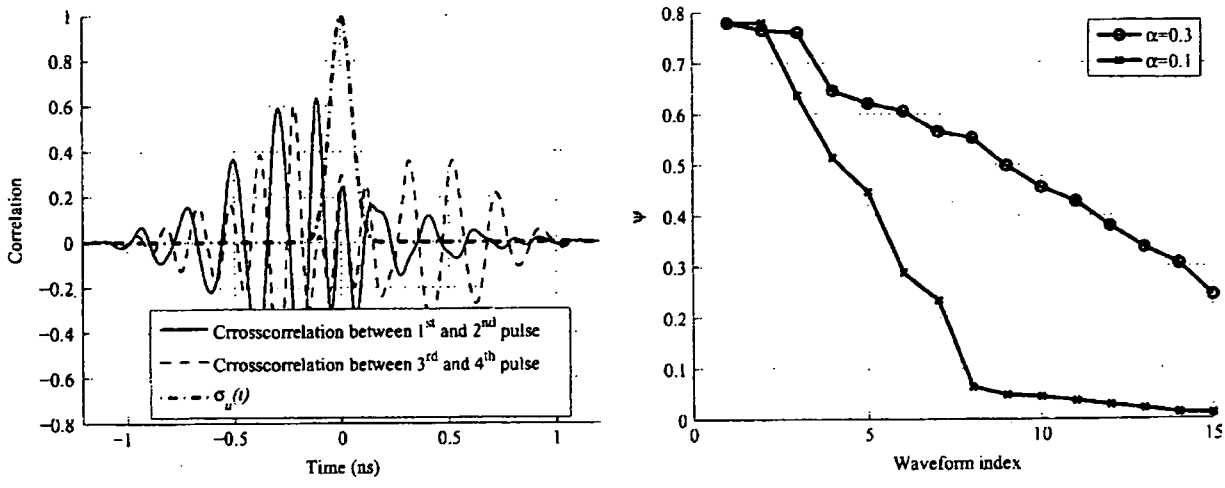

Fig. 12. Designed pulses with robust orthogonality. (a) Pulses' crosscorrelation for $\alpha = 0.3$, (b) ψ attained for different values of α.

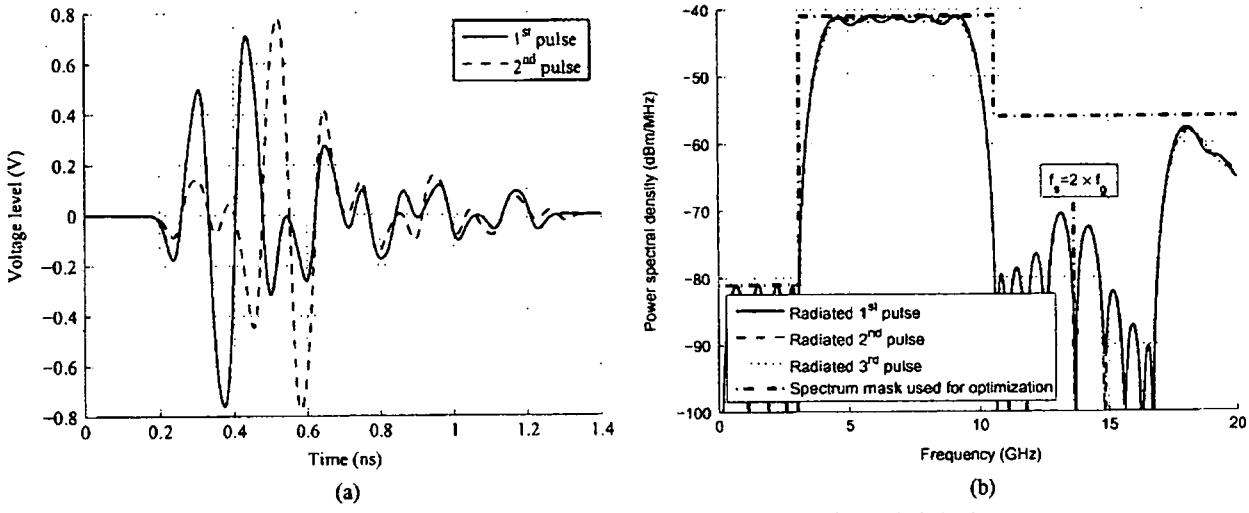

Fig. 13. Designed pulses with $f_s = 2 \times f_g$ and $L = 15$. (a) Pulses' waveforms. (b) Pulses' spectra.

larger α, the number of robustly orthogonal pulses that can be designed with relatively high ψ is lowered.

Therefore, by choosing the value of α, a compromise is made between the interference introduced in reception and the number of designed waveforms with relatively high ψ.

C. Examples of Orthogonal Pulses Design With Suboptimal Sample Rate

Fig. 13 illustrates the successful design of orthogonal pulses with a relatively high ψ using $f_s = 2 \times f_g$. For a given pulse duration (3), ψ achieved is somewhat lower compared to the case when $f_s = 28$ GHz. Furthermore, as shown in Fig. 14, the number of designed orthogonal pulses with relatively high ψ exhibits approximately the same dependence on L, whether $f_s = 2 \times f_g$ or $f_s = 28$ GHz is used. That is, regardless of f_s, approximately the same number of orthogonal pulses with high ψ can be designed for a given L. Moreover, for a given L, pulses with $f_s = 2 \times f_g$ achieve higher ψ at the expense of having higher T_p.

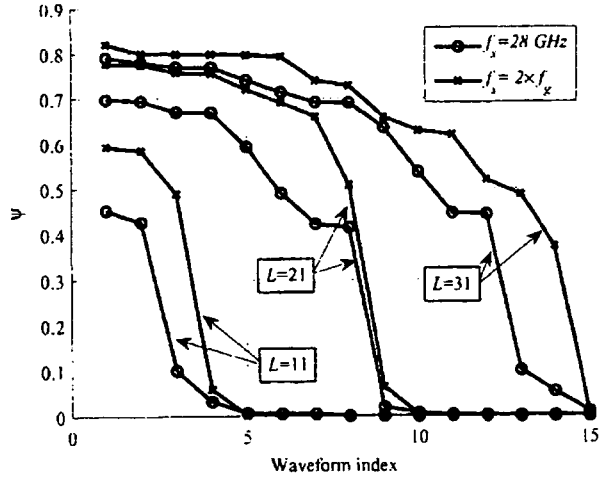

Fig. 14. Achieved ψ with designed orthogonal waveforms for different L and $f_s = 2 \times f_g$.

V. Conclusion

Flexibility and good performance of the method introduced is shown under several orthogonal UWB pulses design scenarios. This method efficiently exploits the given time-bandwidth space defined by pulse duration, sample rate, and EIRP spectrum mask. When a standard problem of the design of multiple orthogonal pulses when radiated is considered, in comparison with similar methods, the method produces a considerably larger number of orthogonal waveforms with high spectral efficiency. The method performs well under conditions of the suboptimal sample rate—it attains the value of ψ for a given T_p which is somewhat below optimal, but produces approximately the same number of orthogonal pulses with relatively high ψ, as when f_s is set to a higher value, and the same value of L is used. Furthermore, it has been shown that the method is capable of producing multiple pulses, the orthogonality of which is robust to the variations of unknown components of the multipath channel. In this case, the value of α is used to make a tradeoff between the number of produced pulses with relatively high ψ and the mean interference between pulses in reception.

Appendix A
Finite Energy Property of the Full-Band UWB Pulses' Crosscorrelation

Consider two full-band UWB pulses: $p_n(t)$ and $p_k(t)$. According to Parseval's theorem, total energy of the $C^g_{k,n}(\tau)$ can be expressed as

$$E_{k,n} = \int_{-\infty}^{+\infty} \left| C^g_{k,n}(\tau) \right|^2 d\tau = \int_{-\infty}^{+\infty} |P_n(f)|^2 |P_k(f)|^2 \, df. \tag{30}$$

Since a majority of the pulses' energy is concentrated under the main lobe of the spectrum mask, (30) can be rewritten as

$$E_{k,n} \approx 2 \times \int_{F_p} |P_n(f)|^2 |P_k(f)|^2 \, df. \tag{31}$$

On the other hand, if both pulses have relatively high ψ, their power spectrum is a good approximation of the given spectrum mask in the F_p

$$|P_n(f)|^2 \approx |P_k(f)|^2 \approx S(f), \quad \forall f \in F_p. \tag{32}$$

Hence, from (31) and (32), we have

$$E_{k,n} \approx E_{n,n} \approx E_{k,k} \approx 2 \times \int_{F_p} S(f)^2 \, df. \tag{33}$$

Therefore, energy of the crosscorrelation function of two pulses with relatively high ψ is approximately equal to the energies of pulses' autocorrelation functions. If we look at (31), we can see that the only way to lower $E_{k,n}$ is either to lower the power spectrum level of one or both of the pulses, lowering in this way their ψ, or to have parts of F_p in which one pulse has a high power-spectrum level (close to the mask) and other does not and vice versa. This again lowers the ψ of one or both pulses and, in addition, lowers their effective bandwidth.

References

[1] L. Michael, M. Ghavami, and R. Kohno, "Multiple pulse generator for ultra-wideband communication using hermite polynomial based orthogonal pulses," in *Proc. IEEE Conf. Ultra Wideband Systems and Technologies, Dig. Papers*, 2002, pp. 47–51.

[2] B. Hu and N. Beaulieu, "Pulse shapes for ultrawideband communication systems," *IEEE Trans. Wireless Commun.*, vol. 4, no. 4, pp. 1789–1797, Jul. 2005.

[3] B. Parr, B. Cho, K. Wallace, and Z. Ding, "A novel ultra-wideband pulse design algorithm," *IEEE Commun. Lett.*, vol. 7, no. 5, pp. 219–221, May 2003.

[4] X. Luo, L. Yang, and G. Giannakis, "Designing optimal pulse-shapers for ultra-wideband radios," in *Proc. IEEE Conf. Ultra Wideband Systems and Technologies*, 2003, pp. 349–353.

[5] X. Wu, Z. Tian, T. Davidson, and G. Giannakis, "Orthogonal waveform design for UWB radios," in *Proc. IEEE 5th Workshop on Signal Processing Advances in Wireless Communications*, 2004, pp. 150–154.

[6] X. Wu, Z. Tian, T. Davidson, and G. Giannakis, "Optimal waveform design for UWB radios," in *Proc. IEEE Int. Conf. Acoustics, Speech, and Signal Processing (ICASSP'04)*. 2004, vol. 4, pp. iv-521–iv-524, vol. 4.

[7] X. Wu, Z. Tian, T. Davidson, and G. Giannakis, "Optimal waveform design for uwb radios," *IEEE Trans. Signal Process.*, vol. 54, no. 6, pp. 2009–2021, Jun. 2006.

[8] J. R. Foerster, Channel Modeling Sub-Committee Report Final, IEEE p802.15-02/368r5-sg3a Tech. Rep., 2002, IEEE P802.15 Working Group for WPAN.

[9] E. W. Weisstein, Eigen Decomposition [Online]. Available: http://mathworld.wolfram.com/EigenDecomposition.html [Online]. Available

[10] J. F. Sturm, "Using SeDuMi 1.02, a MATLAB toolbox for optimization over symmetric cones," *Optimiz. Methods and Software*, vol. 11–12, pp. 625–653, 1999.

Igor Dotlić (M'06) received the B.S.E.E. and M.S.E.E. degrees from the University of Belgrade, Belgrade, Serbia, in 1998 and 2002, respectively, and the Ph.D. degree in communications engineering from the University of Novi Sad, Novi Sad, Serbia, in 2005.

From 1999 to 2005, he was an Associate Researcher at the IMTEL Institute, Belgrade. In 2005, he received the JSPS Fellowship for postdoctoral studies at the Kohno Laboratory, Division of Electrical and Computer Engineering, Yokohama National University, Yokohama, Japan, where he is currently an Postdoctoral Fellow. His research interests include UWB communications and radar, cognitive radio, narrowband and wideband antenna arrays, digital filter design for radar, communications, and medical applications.

Ryuji Kohno (S'81–M'84–SM'02) received the Ph.D. degree in electrical engineering from the University of Tokyo, Tokyo, Japan, in 1984.

He has been a Professor of the Division of Physics, Electrical and Computer Engineering, Graduate School of Engineering, Yokohama National University (YNU), Yokohama, Japan, since 1998. Since October 2002, he has also been President of COE for Creation of Future Social Infrastructure Based on Information Telecommunications Technology at YNU. He was Director of the Advanced Telecommunications Laboratory of SONY CSL during 1998–2002 and is currently a Director of the UWB Technology Institute, Communications Research Laboratory (CRL).

Dr. Kohno has been an Associate Editor of the IEEE TRANSACTIONS ON COMMUNICATIONS since 1994, and IEEE TRANSACTIONS ON INTELLIGENT TRANSPORT SYSTEMS (ITS) since 1999. He was previously an Associate Editor of the IEEE TRANSACTIONS ON INFORMATION THEORY during 1995–1998. He was the Chairman of the IEICE Professional Group on Spread Spectrum Technology during 1995–1998 of ITS during 1998–2000, and currently for Software Defined Radio (SDR). In his academic activities, he was elected a Member of the Board of Governors of the IEEE Information Theory Society in 2000 and 2003. He has contributed toward organizing many international conferences, such as Chair-In Honor of the 2002 International Conference of Software Defined Radio (SDR'02), as TPC Co-Chair of the 2003 International Workshop on UWB Systems (IWUWBS2003), and as General Co-Chair of the 2003 IEEE International Symposium on Information Theory (ISIT'03).

Channel Modeling and Signaling of Medical Implanted Communication Systems and a Step to Medical ICT

Kazunari Tai, Hiroki Harada, Ryuji Kohno
Division of Physics, Electrical and Computer Engineering, Yokohama National University
79–5 Tokiwadai, Hodogaya, Yokohama, 240–8501, Japan.
Tel.: +81-45-339-4116 Fax: +81-45-338-1176
E–mail: {kazunari,hhiroki}@kohnolab.dnj.ynu.ac.jp, kohno@ynu.ac.jp

***Abstract*—Recently, the use of wireless communications devices in the field of medical implants has received great deal of concern due to miniaturization of electronic circuits. By means of transmitting vital data such as blood pressure, blood glucose level and pulse, we can observe the body condition and detect any possible problems in the human body at anytime and anywhere. These devices can help doctors to diagnose and cure diseases.**

For wireless communications, in the case of inside or between inside and outside of the human body, channel propagation considerably differs more than in freespace. So, it is necessary to construct a new channel model of the human body.

In this paper, we analyze wideband channel characteristics in the body based on the measurements and the theory of electromagnetic wave propagation. Based on the measured data, we propose a new frequency domain channel model in the body by using Zero-Pole parameters. We show that the generated channel and the measured channel have similar statical properties by analyzing autocorrelation function of frequency response, power delay profile and cumulative distribution function of power.

I. Introduction

Today, semiconductor technology and circuits technology are quickly evolving. They are resulting in smaller devices and longer-lasting batteries. Furthermore, wireless communication has been developed with nano-size devices by these technologies. These advances have made possible to implant a network of bio-sensors inside the human body for health monitoring purposes. To monitor bio-sensors inside the human body, we can get the real-time information of activity, diet, medications and so on. This technology has been interesting due to the potential to improve a person's quality of life.

In order to design wireless communication systems inside the human body, a propagation channel model plays a very important role. It has been investigated that there are particular effects such as losses involved in the form of absorption of EM wave power by the tissue and many multiple reflective paths due to various tissue materials when signals travel from a transmitter to a receiver inside the human body [1–5]. However, these theoretical analyses are not enough to construct the propagation channel model because it's necessary to consider the probabilistic model due to the individual specificity of tissues and the difference of positions of transceiver. Therefore, generally, conventional channel models such as the indoor multipath fading model have been constructed based on results of propagation measurements [6].

In this paper, we analyze wideband channel characteristics in the body based on the measurements and the theory of electromagnetic wave propagation. Based on the measured data, we propose a new frequency domain channel model in the body by using Zero-Pole parameters. We show that the generated channel and the measured channel have simular statical properties by analyzing autocorrelation function of frequency response, power delay profile and cumulative distribution function of power.

This paper is organized as follows. In Section 2, some basic characteristics of EM wave propagation and properties of dielectic materials which involve the human body tissue are described. Then, in Section 3, measurement of radiowave propagation inside of the body is introduced. Our proposed channel model and its characteristics are presented in Section 4 and Section 5, respectively. Finally, conclusions are drawn.

II. Radiowave Propagation in a Medium

A. Propagation of Electromagnetic Waves in Dielectric Materials

Maxwell's solution in free space is described, however, we must deal with it's solution in lossy medium because of non-zero conductivity and higher permittivity in human body tissues . In lossy medium, permittivity ε is replaced by the complex permittivity $\varepsilon - j\frac{\sigma}{\omega}$. Now, we consider a plane wave which is travelling in the positive z direction, with polarisation in the x direction [7], then,

$$E_x = Ak^2e^{-jkz} = E_0e^{-jkz}, \quad \text{(1a)}$$

$$H_y = A(\omega\varepsilon - j\sigma)ke^{-jkz} = H_0e^{-jkz}, \quad \text{(1b)}$$

$$E_y = Ez = Hx = Hz = 0, \quad \text{(1c)}$$

$$k = \sqrt{\omega^2\mu\varepsilon - j\omega\mu\sigma}, \quad \text{(1d)}$$

where μ is permeability and wave impedance is obtained,

$$\frac{E_x}{H_y} = \frac{E_0}{H_0} = \sqrt{\frac{\omega\mu}{\omega\varepsilon - j\sigma}} = Z_0 \ . \quad (2)$$

The impeadance is complex in a lossy medium and then phase difference occurs. Additionally, the propagation constant is also complex, therefore electric and magnetic fields are

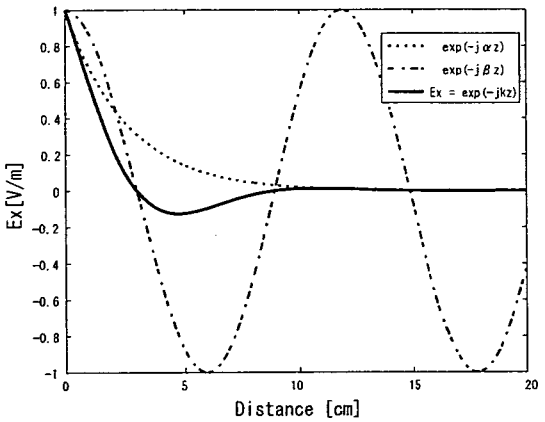

Fig. 1. Attenuation of EM wave in a lossy medium.

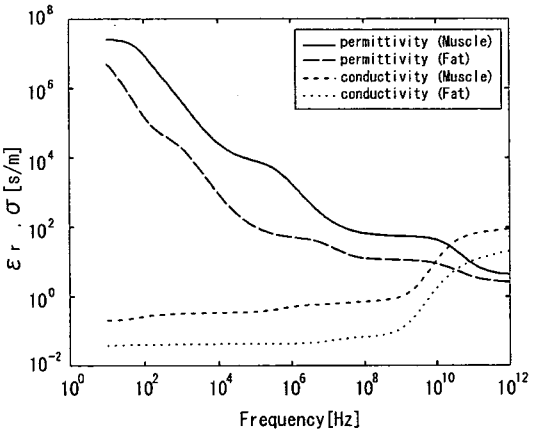

Fig. 2. Dielectric parameters of muscle and fat.

attenuated while traveling in Fat as shown in Fig. 1. The permittivity of Fat is 7.5 and the conductivity is 0.15S/m at 1.0GHz. Propagation constant k is generally, seperated into real component and imaginary component as follows [8],

$$k = \beta - j\alpha, \tag{3}$$

$$\alpha = \omega\sqrt{\mu\varepsilon}\sqrt{\frac{1}{2}\left(\sqrt{1+\left(\frac{\sigma}{\omega\varepsilon}\right)^2}-1\right)}, \tag{4}$$

$$\beta = \omega\sqrt{\mu\varepsilon}\sqrt{\frac{1}{2}\left(\sqrt{1+\left(\frac{\sigma}{\omega\varepsilon}\right)^2}+1\right)}, \tag{5}$$

where α is the attenuation constant and β is the phase constant.

B. Human Body Tissue

A human body consists of various organs with complex structures. Furthermore, each organ has different characteristics of conductivity and permittivity.

We should consider the frequency band when we try to communicate with implanted devices because of the frequency depencency of these parameters. Generally, if the tissue has higher percentage of water content, then the relative permittivity and conductivity are high. Therefore, EM wave attenuation will be significant. The measurement of dielectric properties is well known [9]. The method measures dielectric properties of human body tissue in the frequency range from 10 Hz to 100 GHz. On the other hand, there is well known dispersions in the dielectric spectrum of biological materials and their expression as a summation of terms corresponding to the main polarisation mechanism. The spectrum extends from 10 Hz to 100 GHz and show four dispersion regions. The complexity of the structure and composition of biological material such that each dispersion region is broadened by multiple contributions to it, should be described by a Cole-Cole expression [10]. Fig. 2 shows dielectric properties of muscle and fat tissue calculated by the Cole-Cole equation as follows,

$$\varepsilon(\omega) = \varepsilon_\infty + \sum_{n=1}^{4}\frac{\Delta\varepsilon_n}{1+(j\omega\tau_n)^{(1-\alpha_n)}} + \frac{\sigma_i}{j\omega\varepsilon_0}. \tag{6}$$

III. Measurement of Radiowave Propagation Inside of the Body

A. Antenna

In a lossy matter the insulated wire antenna can be treated as a coaxial waveguide [11]. The lossy matter acts as the outer conductor. This waveguide has a propagation constant γ which is influenced both by the dielectric properties of the insulation, and by the properties of the surrounding matter. In [12] an approximate solution to the input impedance of the insulated wire antenna is presented. The impedance of the wire antenna is defined as $Z_{wire} = Z_0' \coth\gamma l$, where l is the length of the wire. γ is the complex propagation constant approximated by

$$\gamma \approx \sqrt{-\omega^2\mu_2\varepsilon_2}\left(1 - \frac{j\pi/4 + \ln(0.89\sqrt{2}\frac{a_{out}}{\delta})}{\ln\frac{a_{out}}{a_{in}}}\right)^{1/2}. \tag{7}$$

Here μ_2 and ε_2 are the electromagnetic properties of the insulation, a_{out} and a_{in} are the outer and inner radii of the insulator and δ is the skin depth in the surrounding material. The characteristic impedance Z_0' is approximated by

$$Z_0' = \left(\frac{1}{2\pi}\ln\frac{a_{out}}{a_{in}}\right)\frac{\gamma}{j\omega\varepsilon_2}. \tag{8}$$

The skin depth is $\delta = 1/\mathrm{Re}[\gamma_s]$, where γ_s is the complex propagation constant of the surrounding material. The approximation is valid if the propagation constant for the lossy outer medium is much greater than the line propagation constant δ. The approximation is said to be valid if $a_{out}/\delta < 0.1$.

We performed the measurement with a_{out} = 3.5mm using purified water as the insulator. The permittivity of purified water is 50 at 2GHz. The conductivity is 1.0 S/m, which is lower than that of body tissues (1.45 S/m).

B. Measurement Setup

We measured radiowave propagations in the body of a pig. The aim of the experiments was to investigate the statistical frequency charactreistics and the effect caused by the heart motion. The pig was about 90cm (from nose to hip) and about 25 kg. During the experiment it was laying in backwards

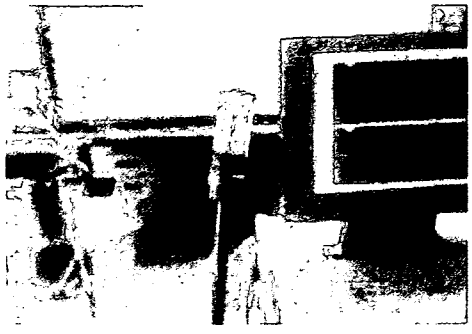

Fig. 3. The Antenna for the experiment

position over the bed. The pig was under anesthesia and on a mechanical ventilator during the experiment.

1) Incision:
   Cutting the abdomen skin of the pig in the middle with a cautery knife. The cut range along y axis was from the diaphragm to the lower part of the small intestine.
2) Insertion:
   Inserting the antennas between the tissues of the pig in a co-polarized position. The inserted positions are shown in Fig. 4. The x-marks in Fig. 4 indicate the inserted points of the port 1. Eight set of measurements were performed as shown by from A to I in Fig. 3. In every set, the measurements were performed six times at a different distance between 2 ports. The port 1 was fixed, the port 2 was moved changing the distance after the measurement. The distances between ports were from 2cm to 12cm at 2cm intervals. The inserted depth was 8cm from the pig skin, respectively. When the port 2 was moved, it was pulled out of the body, before it was inserted again in a different position. In a set A to D of Fig. 4, the port 1 was inserted on the top, bottom, left and right part of the stomach respectively, the port 2 was inserted below (-y direction) the port 1. In a set E to H, the port 1 was inserted on the lower part of the small intestine and the port 2 was inserted above (+y direction) the port 1.
3) Suture:
   Suture the abdomen of the pig with a surgical thread to close the cut caused by the incision.
4) Measurement:
   Measuring S-parameter using Agilent E8363B vector network analyzer (VNA). The frequency range was from 10MHz to 10GHz with a frequency span of 10MHz (801 points).
5) Calculation:
   Calculating $H(f,d)$ from mesured S-parameters as follows

$$H(f,d) = \frac{S_{21}}{(1-S_{11})*(1-S_{22})}. \quad (9)$$

IV. Channel Modeling

In this section, we present a channel modeling method for implant communications, especially, we describe a Zero-Pole model as a novel modeling method. This model is

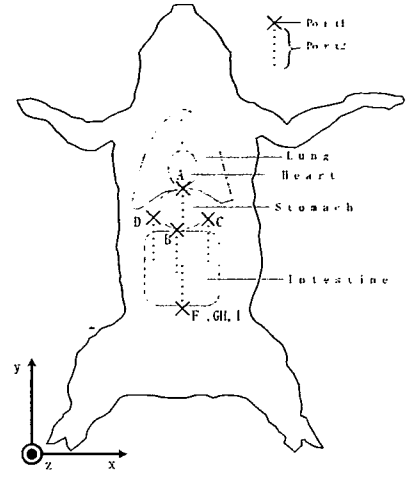

Fig. 4. position of inserted antennas in the pig

able to generate realizations and express stochastic frequency dispersion.

We show the generated channel and the measured channel have simular statistical properties by analyzing the autocorrelation function for frequency response, power delay profile and cumulative distribution function of power.

A. Frequency Dependent Path Loss

Generally, frequency-dependent pathloss free space at a distance d is given by[6],

$$\hat{PL_{air}}(f,d) = \frac{1}{2} PL_0 \eta_{TX_{ant}}(f) \eta_{RX_{ant}}(f) \left(\frac{d}{d_0}\right)^{-n} \left(\frac{f}{f_c}\right)^{-2(\kappa+1)}, \quad (10)$$

where $PL_0 = PL(f_c, d_0)$ is the nomalization constant, $\eta_{TX_{ant}}(f)$ and $\eta_{RX_{ant}}(f)$ are respectively frequent dependent transmit and receive antenna efficiency. Note that this reverts to the conventional picture of energy spreading out equally over the surface of a sphere when we set $n = 2$, and $\kappa = 0$.

We modify Eq. (10) for lossy medium as follows

$$\hat{PL_{body}}(f,d) = \hat{PL_{air}}(f,d) \mathrm{e}^{-2\alpha(f)d} \quad (11)$$

note that each coefficient (PL_0, n, κ) has a different value from a case on free space. Where $\alpha(f)$ is the attenuation constant given by Eq. (4). The value of α is set from 2/3 of the permittivity of muscle for the reason that the proportion of the tissue of high water content to the one of low water content is 2:1 in a human body[9]. Although $\alpha(f)$ is an average characteristic a human body has it is in fact, an unequal structure for various tissues. Furthermore, it is difficult to consider all tissue passed through by radiowave between antennas(including 3D reflection effect), this becomes an indeterminaion component. Thus, we give a variation function $V(f)$ to compensate those indeterminaion components,

$$\begin{aligned} PL_{body}(f,d) &= \hat{PL_{body}}(f,d) V(f) \\ V(f) &= Av(f). \end{aligned} \quad (12)$$

Here A is a Gaussian-distributed random variable with zero mean and standard deviation σ_0 in dB (like a shadowing

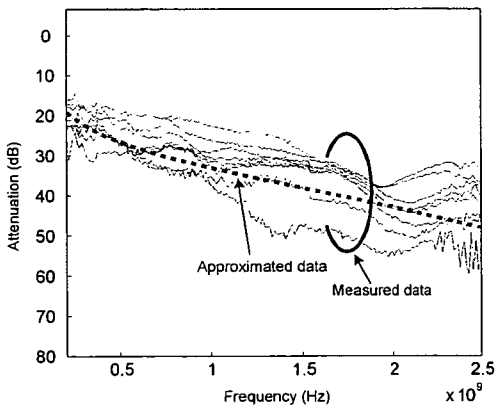

Fig. 5. Attenuation of the channel on measured data ($H(f,d)$) and approximated data ($\hat{H}_0(f,d)$).

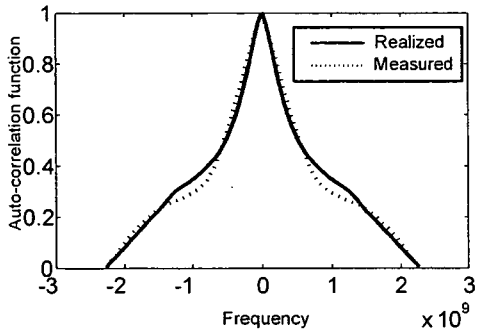

Fig. 6. Normalized autocorrelation function for frequency response

efficience on air environment). This derives from the fact that different α causes a different pathloss linearly in log domain at a same distance. v(f) is a variation function which has frequency dependence. v(f) will be modeled in next section.

Considering phase coefficient $\beta(f)$ and subtracting antenna effect, we derive the frequency response of the channel as follows

$$\begin{aligned} H(f,d) &= \hat{H}_0(f,d)Av(f) \\ \hat{H}_0(f,d) &= \frac{\hat{PL_{body}}(f,d)}{\sqrt{\eta_{TX}(f)\eta_{RX}(f)}}\, e^{-j\beta(f)d} \\ &= \sqrt{\frac{1}{2}PL_0(\frac{d}{d_0})^{-n}(\frac{f}{f_c})^{-2(\kappa+1)}}\, e^{-(\alpha(f)+j\beta(f))d} \end{aligned} \tag{13}$$

where $v(f)$ includes phase component.

Fig. 5 shows the measured data ($H(f,d)$) and the approximated data ($\hat{H}_0(f,d)$) of frequency response. The channel yields n = 1.2 , κ = -0.2 , PL_0 [dB] = 2.3 , Tissue =2/3 Muscle ,σ_0 [dB] = 3.1 and σ_f [dB] = 2.3 (at f_c =100MHz and d_0 =20mm)

B. Zero-Pole Model

The modeling of $v(f)$ is able to generate H(f,d). The procedure for making $v(f)$ using zero-pole model is as follows: zero-pole extraction, probability distribution estimation and generating realizations.

C. Zero-Pole Extraction

Equation error method is an algorithm to identify the best model from the data. This finds b and a in

$$\min_{b,a} \sum_{k=1}^{L} W(k) \left| D(k) - \frac{B(k)}{A(k)} \right|. \tag{14}$$

Here $A(\omega(k))$ and $B(\omega(k))$ are the Fourier transforms of the polynomials a and b,respectively, at the frequency ω_k, $D(k)$ is an arbitrary desired frequency response, and $W(k)$ is a weight function, and L is the number of frequency points (the length of D and W). This algorithm is a based on Levi[13]. Damped Gauss-Newton method is used for iterative search [14], with the output of the first algorithm as the initial estimate. This solves the direct problem of minimizing the weighted sum of the squared error between the actual and the desired frequency response points.

Every polynomial can be characterized by its roots plus a scale factor, therefore, Nth/Nth order transfer function could be factorised

$$\begin{aligned} H(z) &= H_0 \frac{z^N + b_{N-1}z^{N-1} + \ldots b_1 z^1 + b_0}{z^N + a_{N-1}z^{N-1} + \ldots a_1 z^1 + a_0} \\ &= H_0 \frac{(z-q_1)(z-q_2)\ldots(z-q_N)}{(z-p_1)(z-p_2)\ldots(z-p_N)}. \end{aligned} \tag{15}$$

Here, q_i is zero, p_i is pole. In equation 15, we substitute $z = e^{j\omega T}$

$$H(e^{j\omega T}) = H_0 \frac{\prod_{i=1}^{N}(e^{j\omega T} - q_i)}{\prod_{i=1}^{N}(e^{j\omega T} - p_i)}. \tag{16}$$

D. Generating Realization

Next, we will discuss the stochastic modeling of the zero and pole. Assuming that the amplitude of zeros and pole have normal distribution N[μ_q, σ_q] and N[μ_p, σ_p]. The angle distributions are of uniform distribution.

The average and standard diviation of zero is μ_q = 0.481 , σ_q = 0.114 and of pole is μ_p = 0.205 , σ_p = 0.082.

Generating poles and zeros from random number which have a normal distribution N[μ_q, σ_q] and N[μ_p, σ_p], v(f) in (13) is generated from(15).

V. Performance Evaluation

A. Frequency Domain

We measure the normalized auto-correlation function of realised and measured frequency responses to be able to find the efficacy of the model as shown in Fig. 6. Using the normalized auto-correlation function of frequency responses, we are able to get an estimate of the frequency range for which the channel can be assumed to be flat. Fig. 7 is the Cumulative distribution function of power spector density. The results show that the realised responses are comparable to the measured data.

B. Time Domain

The impulse response in time domain is used as a description of a channel response. We can obtain the impulse

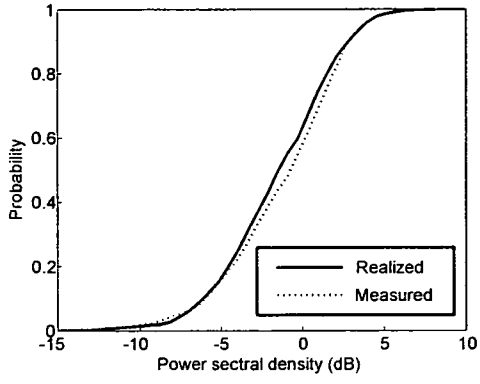

Fig. 7. Cumulative distribution function of power spector density

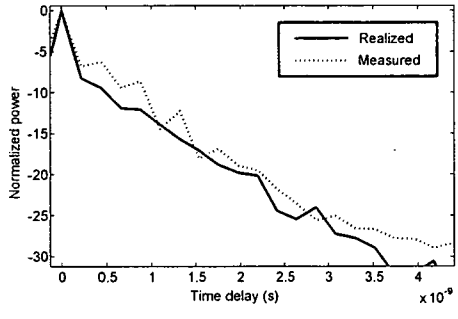

Fig. 8. Average delay profile of the channel

response of a channel from frequency response by inverse Fourie transform:

$$H(f,t) = \int_0^\infty h(\tau,t)\exp(-j2\pi f\tau)\,d\tau \quad (17a)$$

$$h(\tau,t) = \int_{-\infty}^\infty T(f,t)\exp(j2\pi f\tau)\,df \quad (17b)$$

The average delay profile is used to find the efficacy of the model in time domain. The average delay profile is the expected power per unit of time received with a certain excess delay. It is obtained by averaging a large set of impulse responses. Fig. 8 shows the average delay profile of measured and realized data. The results show that the Zero-Pole model generates responses comparable to the statistics of the measured time domain responses. Fig. 9 shows the cumulative distribution functions of the realised impulse response and measured data. The results are comparable.

VI. Conclusions

In this paper, we analyze wideband channel characteristics in the body based on the measurements and the theory of EM wave propagation and properties of dielectic materials. We measure S_{21} parameters between two antennas inserted in 48 different points of pig bodies. Experimental results show that severe attenuation in high frequency band and smaller time delay take place in contrast to the case of free-space propagation. Meanwhile, we also show the most appropriate

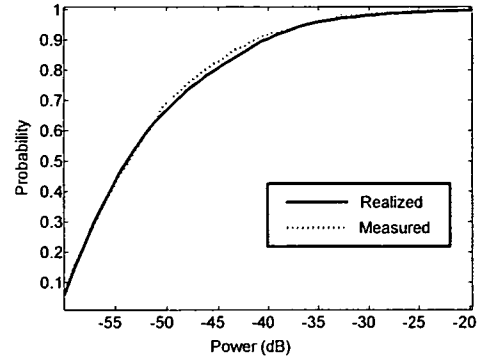

Fig. 9. Cumulative distribution function of power in time domain

frequency band for human body channel considering the channel capacity.

Based on the measured data, we propose a novel frequency domain channel model in the body by using Zero-Pole parameters. This model is able to generate frequency domain responses and express stochastic frequency dispersion. We show that generated channel and the measured channel have similar statistical properties by analyzing the autocorrelation function of frequency response, power delay profile and cumulative distribution function of power.

References

[1] A. J. Johansson, "Wireless Communication with Medical Implants: Antennas and Propagation", Sweden, Lund University, 2004, Ph.D. thesis.

[2] S. K. S. Gupta, S. Lalwani, Y. Prakash, E. Elsharawy, L. Schwiebert, "Towards a propagaion model for wireless biomedical applications," IEEE International Conference on Communications (ICC 2003), May. 2003.

[3] W. G. Scanlon, J. B. Burns, and N. E. Evans, "Radiowave Propagation from a Tissue-Implanted Source at 418 MHz and 916.5 MHz,"

[4] P. Valdastri, A. Menciassi, A. Arena, C. Caccamo, and P. Dario, "An Implantable Telemetry Platform System for In Vivo

[5] J. Kim, Y. Rahmat-Samii, "Low-profile antennas for implantable medical devices: optimized designs for antennas/human interactions", IEEE Antennas and Propagation Society International Symposium, vol.2, pp.1331-1334, June 2004.

[6] A. F. Molisch, K. Balakrishnan, C. Chong, S. Emami, A. Fort, J. Karedal, J. Kunisch, H. Schantz, U. Schuster, K. Siwiak, "IEEE802.15.4a channel model - final report", IEEE P802.15 Wireless Personal Area Networks, Sept. 2004.

[7] Y. Mushiaki "Antenna and Wave Propagation," Corona Publishing, 2001.

[8] T. Ohmori, "Bio Electromagnetic Engineering and Application ," Fujitec Corporation

[9] C. Gabriel, S. Gabriel, "Compilation of the dielectric properties of body tissues at RF and Microwave Frequencies," http://www.brooks.af.mil/AFRL/HED/hedr/reports/dielectric/home.html

[10] K. S. Cole and R. H. Cole, "Dispersion and absorption in dielectrics : 1. Alternating current characteristics.," *Journal of Chemical Physics*, Apr. 1941.

[11] R. W. P. King and S. G. S., Antennas in Matter. the MIT Press, 1981.

[12] R. C. Fenwick and W. L. Weeks, "Submerged antenna characteristics," IEEE Trans. on Antennas and Propagation, vol. 11, May 1963.

[13] Levi, E.C., "Complex-Curve Fitting," IRE Trans. on Automatic Control, Vol.AC-4 (1959), pp.37-44.

[14] Dennis, J.E., Jr., and R.B. Schnabel, Numerical Methods for Unconstrained Optimization and Nonlinear Equations, Prentice-Hall, 1983.

[15] B. Sklar, "Rayleigh fading channels in mobile digital communication systems. Part I: Characterization," *IEEE Communication Magazine.*, vol. 35, pp. 94-102, Jul. 1997.

An Analysis of Interference Mitigation Capability of Low Duty-Cycle UWB Transmission in The Presence of Wideband OFDM Systems

Keisuke Sodeyama†, Koji Ishibashi‡, Ryuji Kohno†

†Division of Physics, Electrical and Computer Engineering, Yokohama National University
79–5 Tokiwadai, Hodogaya-ku, Yokohama, 240–8501, Japan.
‡Department of Electrical and Electronic Engineering, Faculty of Engineering, Shizuoka University
3–5–1 Johoku, Naka-ku Hamamatsu, Shizuoka, 432–8561, Japan.

E–mail: sodeyama@kohnolab.dnj.ynu.ac.jp, koji@ieee.org, kohno@ynu.ac.jp

Abstract— **Ultra wideband (UWB) radio communication has gained much attention such as a future communication technology. UWB radio devices must equip the interference mitigation technology since the radio band of the UWB radio systems overlaps that of other radio systems such as world wide interoperability for microwave access (WiMAX), 4th generation mobile cellular systems (4G), and field pickup unit (FPU).**

In this paper, the performance of wideband systems using orthogonal frequency division multiplexing (OFDM) over the coexistence environment is analyzed. In order to analyze the interference mitigation capability of *low duty-cycle* (LDC) protocol with impulse-based UWB radio system (LDC-UWB). Mutual collision probability between wideband OFDM systems and LDC-UWB systems is investigated and two states Markov collision model is proposed. Also, the frame error rate (FER) of wideband OFDM systems is discussed by using computer simulations. Moreover, we statistically show that interference of UWB signals can be modeled as the white Gaussian noise.

Keywords— **low duty-cycle, LDC-UWB, two states Markov collision model, interference mitigation technique, wideband OFDM**

I. Introduction

Recently, ultra wideband (UWB) radio communication has gained much attention such as coexistence with other radio systems because of its low power spectrum density equivalent to noise level [1]. However, UWB radio communications may inherently degrade the performance of the other radio systems since the radio band of the UWB radio systems overlaps that of other radio systems such as worldwide interoperability for microwave access (WiMAX), 4^{th} generation mobile cellular systems (4G), and field pickup unit (FPU). Therefore, it is essential for UWB radio communications to equip interference mitigation techniques, *detect and avoid* (DAA) and *low duty-cycle* (LDC).

The device with DAA can detect the signals from existing victim systems and avoid the interference for them. High data rate UWB radio communication with DAA has been studied in the literature [2],[3]. Originally, LDC protocol has been studied to reduce energy consumption [4]. LDC protocol is extended in order to reduce the average interference to other systems by lowering the pulse repetition interval or pulse occupation time. Moreover, in UWB wireless as hoc network, LDC protocol has been studied to improve the near/far power disparities or pulse-on-pulse interference of multiple access [5]-[7]. Low data rate UWB radio communication with LDC protocol such as IEEE 802.15.4a has been studied since wireless sensor network requires long battery life and low cost rather than high data rate communication. Although LDC protocol promises that the average interference to other radio systems can be suppressed UWB radio systems still interfere with other radio systems even with LDC protocol.

In this paper, we focus on the coexistence environment of UWB radio systems and wideband systems based on orthogonal frequency division multiplexing (OFDM) such as 4G and WiMAX. In order to analyze the interference mitigation capability of LDC protocol with impulse-based UWB radio system (LDC-UWB), the performance of wideband OFDM system over the coexistence environment is studied. Specially, mutual collision probability between wideband OFDM systems and LDC-UWB systems is investigated and two state Markov collision model is proposed. Also, the frame error rate (FER) of wideband OFDM systems is discussed by using computer simulations.

The rest of this paper is organized as follows. In Section II, network models considered throughout

Type of UWB system	Impulse-based UWB
Center Frequency f_c	4.0 GHz
Bandwidth	2 GHz
Data rate	> 1 Mbits/s
Pulse repetition interval	3.9 MHz, 15.6 MHz
Pulse width	0.5 ns
Duty-Cycle	0.1, 1, 5, 10, 50, 100 %
Tx (or Rx) slot length	1 ~ 1,001 ms
Sleep period after Tx (or Rx)	1,000 ~ 0 ms
UWB frame length	2,002 ms

Tab. 1. Major parameters of UWB systems

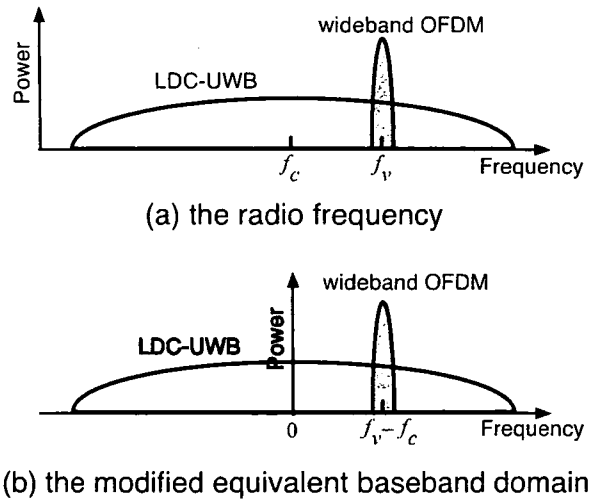

Fig. 1. Frequency spectra of the LDC-UWB system and the wideband OFDM system in: (a) the RF domain and (b) the modified equivalent baseband domain.

the paper are presented. Two states Markov collision model is discussed in Section III. Simulation results and discussion are given in Section IV. Finally, the conclusions are drawn in Section V.

II. Network Models

A. UWB SYSTEM NETWORK MODEL

The major parameters of UWB radio systems are listed in Tab. 1. In this paper, low data rate UWB radio system is assumed such as IEEE 802.15.4a and sensor network and thus its data rate is below 1 MHz bits per second (bps). Also, the pulse repetition interval is 3.9 MHz or 15.6 MHz which is compliant with IEEE 802.15.4a. Here, the pulse repetition interval (PRF) is defined that pulse repetition interval at the range of the transmit slot length of LDC-UWB device. Although impulse radio signals of UWB communications are not exactly Gaussian, their interference effect to narrowband systems can be approximated as a white Gaussian noise [8]. However, LDC-UWB systems are changing pulse repetition interval or pulse occupation time. Therefore, the LDC-UWB signals cannot be approximated as a white Gaussian noise.

B. MODIFIED EQUIVALENT BASEBAND UWB SYSTEM NETWORK MODEL

In this paper, UWB signal interference is modeled both of a white Gaussian noise and a modified equivalent baseband system [9]. UWB radio communication is accepted at the radio frequency from 3.4 GHz to 10.6 GHz in Japan. At the computer simulation, using these frequency band is difficult. Moreover, the time of computer simulation has increased since sampling frequency become significantly high and LDC protocol is included. Therefore, the simulation model implemented a modified equivalent baseband system in order to speed up the simulation. Fig. 1 illustrates the spectral relation between the culprit LDC-UWB system and the wideband OFDM system, whose center frequencies are f_c and f_v, respectively, in the radio frequency (RF) domain. The victim system is shifted from f_v to $f_v - f_c$ in order to tune the center frequency to specific frequency of the UWB signal in the modified equivalent baseband domain.

C. LDC-UWB SYSTEM NETWORK MODEL

LDC protocol is extended in order to reduce the average interference to other systems by lowering the pulse repetition interval or pulse occupation time.

LDC protocol [10] considered throughout the paper is briefly explained. In this protocol, every UWB radio devices wake for only a short time to communicate with other devices and timing schedule of UWB radio devices is not available at each devices. Thus, in order to establish a communication link, access controller (AC) is introduced. The wireless network based on LDC protocol must have one AC device, which may be allowed relatively high power consumption and high duty-cycle (HDC) compared with those of non-AC devices. AC can receive messages from all UWB radio devices belonging to its own network. Moreover, AC has the timing schedule of every devices. Note that this protocol is good for applying indoor applications since AC device should operate with the power line because of its high power consumption and high duty-cycle. Fig. 2 is illustrated as an example of the LDC protocol with UWB radio devices A and B, where, the duty-cycle is about 0.1 %, both UWB radio devices transmit (T_x) and receive (R_x) time slot length are 1 ms, and AC has 2,002 ms receive time slot. The duty-cycle is defined as follows:

$$DC_{UWB} = \frac{2T_{s-UWB}}{T_{f-UWB}}, \quad (1)$$

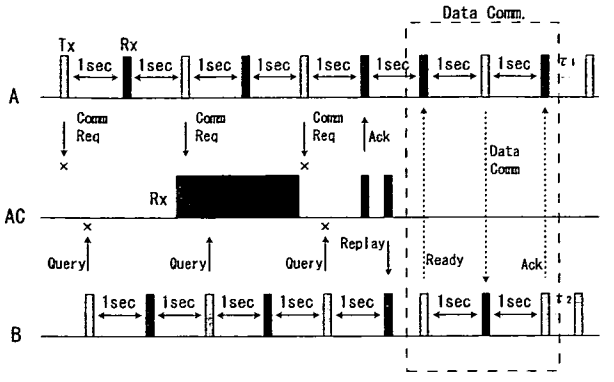

Fig. 2. LDC protocol: an example of duty-cycle = 0.1 %.

Bandwidth	101.5 MHz
Data rate objective	> 100 Mbits/s
Number of sub-carriers N_c	768
Sub-Carrier spacing F_s	131.8 kHz
OFDM symbol duration T_s	7.585 μs
Total OFDM symbols duration T_s'	9.259 μs
Number of OFDM symbols per frame N_s	54
OFDM frame length T_{fr}	500 μs
Symbol mapping	QPSK

Tab. 2. Major parameters of wideband OFDM systems

where DC_{UWB} is duty-cycle of UWB, $2T_s - UWB$ is transmit/receive (T_x/R_x) slot length, $T_f - UWB$ is frame length of UWB. $T_f - UWB$ is fixed 2,002 ms. For example, duty-cycle 0.1 % is defined that T_x and R_x of UWB radio devices are 1 ms and total sleep period per frame is 2,000ms, duty-cycle 50 % is defined that Tx and Rx are 500 ms and total sleep period per frame is 1002 ms.

Device A keep sending a communication request (Comm. Req.) message to AC until the Ack message is received from AC, where Comm Req message includes it is own timing schedule and request to device B. Simultaneously, device B keep sending a Query message until Replay message from AC device is received as illustrated in Fig. 2, where Replay message includes the timing schedule of device A and its request to device B. Then, device B adjusts its own timing schedule to that of device A and device B sends a Ready message to device A directly. Then, a communication link between device A and device B is established.

D. OFDM SYSTEM MODEL

The block diagram of the wideband OFDM system is shown in Fig. 3. Major parameters of wideband OFDM systems are listed in Tab. 2 (c.f., [10]). In this paper, the bandwidth of the wideband OFDM system such as 4G and WiMAX is about 100 MHz and thus its data rate is 100 MHz bps. Then, by considering the equivalent baseband model is employed. Thus, the interference of the UWB signals is introduced as follows. The UWB signal is added to the transmitted OFDM signal (see Fig. 3). After that, the received signals are passed through the low pass filter (LPF) of the wideband OFDM system.

III. TWO STATES MARKOV COLLISION MODEL

As mentioned adobe, the frame length of LDC-UWB system is assumed 2,002 ms since each Tx and Rx is

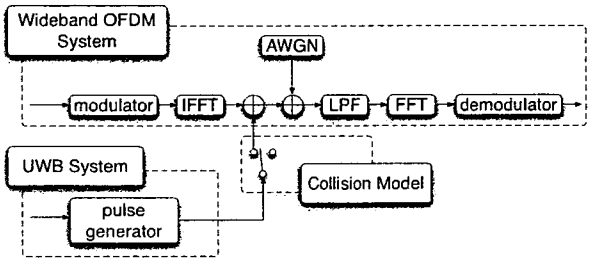

Fig. 3. The block diagram of the wideband OFDM system.

500 ms and its sleep period is respectively 501 ms (about duty-cycle of LDC-UWB is 50 %). The frame length of wideband OFDM system is assumed 500 μs. Fig. 4 shows the mutual collision probability between the wideband OFDM system and LDC-UWB system calculated by computer simulations, when duty-cycle of LDC-UWB is 50 %. Mutual collision probability is defined as the probability of overlapping frames of wideband OFDM system and LDC-UWB system.

From Fig. 4, the mutual collision probability can be divided into two states:

- full collision
- no collision.

For the reason that the frame length of LDC-UWB is much longer than that of the wideband OFDM. Hence, we consider the two states Markov collision model as the mutual collision model between the LDC-UWB system and the wideband OFDM system in this paper.

IV. SIMULATION RESULTS

Although LDC protocol promises that the average interference to other radio systems can be suppressed, LDC-UWB radio systems still interfere with other radio systems even with LDC protocol. Moreover, when UWB radio devices (or users) are increased, the interference to wideband OFDM may be increased even applying lower duty-cycle.

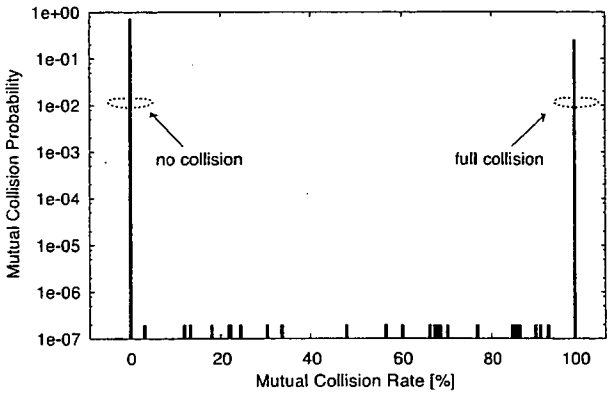

Fig. 4. The mutual collision probability between wideband OFDM system and LDC-UWB system, when duty-cycle of UWB is 50 %.

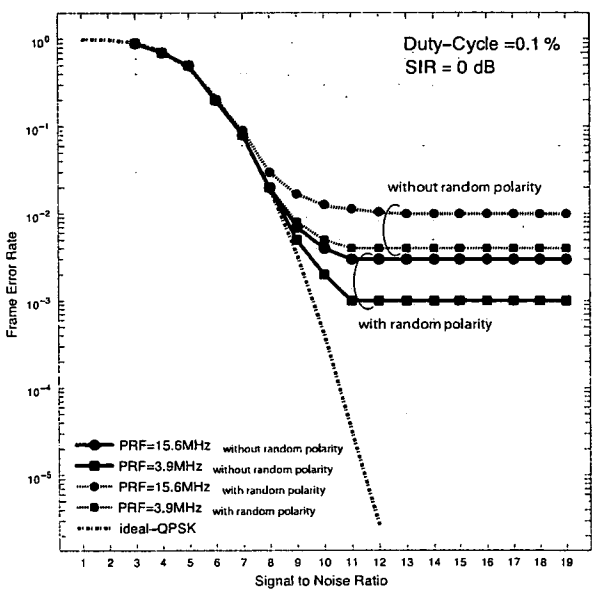

Fig. 5. The FER of the wideband OFDM systems over AWGN channel with the interference by LDC-UWB system when SIR = 0 dB and duty-cycle = 0.1 %.

First, the FER of the wideband OFDM systems over additive white Gaussian (AWGN) channel with the interference by the LDC-UWB. The LDC-UWB signal interference is considered about two types: with random polarity such as plus or minus at random, and without random polarity such as constant polarity. For the reason that it is simplicity for the devices using the signal without random polarity to design the circuits. However, originally, the signal with random polarity is necessary since when the PRF of LDC-UWB is increased, the frequency spectrum becomes line spectrum. Moreover, IEEE 802.15.4a can be used the modulation with random polarity. Fig. 5 shows the FER of the wideband OFDM system with the interference by the LDC-UWB system when SIR = 0 dB, duty-cycle is 0.1 % and PRF = 3.9 MHz or 15.9

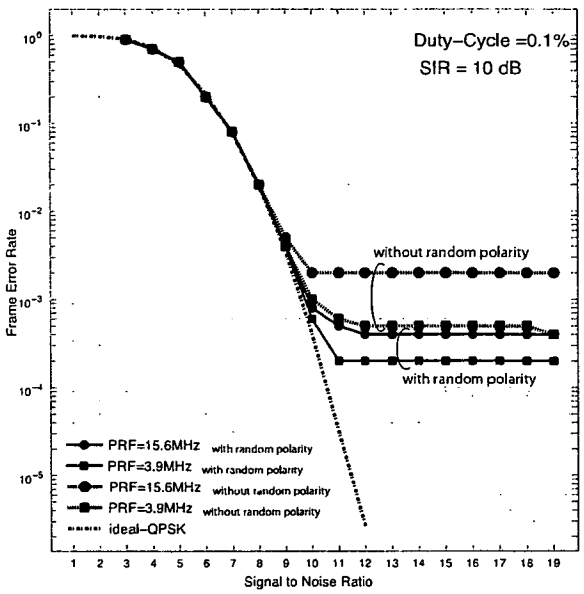

Fig. 6. The FER of the wideband OFDM systems over AWGN channel with the interference by LDC-UWB system when SIR = 10 dB and duty-cycle = 0.1 %.

MHz. Fig. 6 shows the FER of the wideband OFDM system with the interference by the LDC-UWB system when SIR = 10 dB, duty-cycle is 0.1 %, and PRF = 3.9 MHz or 15.9 MHz. Here, signal to interference ratio (SIR) is defined that the wideband OFDM system transmitter signal power to LDC-UWB interference transmitter signal power ratio.

From Fig. 5 and Fig. 6, the FER of wideband OFDM system with LDC-UWB interference by random polarity is superior to that of the LDC-UWB interference without random polarity. For the reason that the LDC-UWB interference without random polarity is increased interference since constant signal polarity is added to wideband OFDM system. Moreover, the LDC-UWB interference without random polarity is occurred the phase rotation. Meanwhile, the LDC-UWB interference with random polarity is denied the each signal polarity. In addition, the phase rotation is reduced by random polarity.

From another viewpoint, the FER of wideband OFDM systems are degraded by the PRF of LDC-UWB systems since the interference pulses are increased PRF = 15.6 MHz. Therefore, the PRF of LDC-UWB systems should be chosen carefully in consideration of the performance required quality of wideband OFDM system and the request of the each LDC-UWB applications.

Secondly, the FER of wideband OFDM system over AWGN channel with the interference by LDC-UWB systems when the duty-cycle of LDC-UWB system is changed. Here, signal to noise rate is fixed 10 dB.

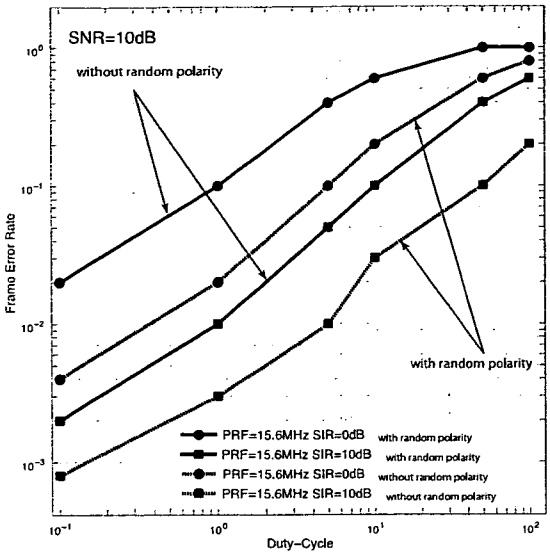

Fig. 7. The FER of the wideband OFDM system with the interference by the LDC-UWB radio devices, when SNR = 10 dB and the pulse repetition interval is 15.6 MHz.

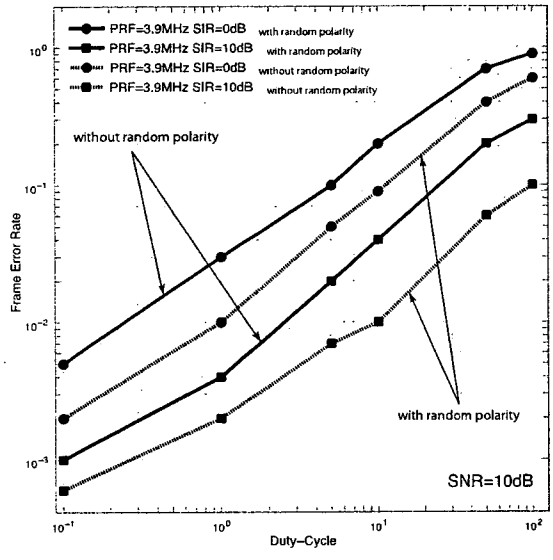

Fig. 8. The FER of the wideband OFDM system with the interference by the LDC-UWB radio devices, when SNR = 10 dB and the pulse repetition interval is 3.9 MHz.

Figure 7 shows the FER of the wideband OFDM systems with the interference by the LDC-UWB radio devices, where SNR is 10 dB, PRF = 15.6 MHz. Figure 8 shows the FER of the wideband OFDM systems with the interference by the LDC-UWB radio devices, where SNR is 10 dB, PRF = 15.6 MHz.

From Figure 7 and 8, the FER of wideband OFDM systems are degraded with increasing of the duty-cycle of LDC-UWB systems. LDC cannot suppress interference to wideband OFDM systems completely. However it can be mitigated moderately without additional complexity such as DAA. Thus, the duty-cycle of LDC-UWB should be chosen carefully in consideration of the performance required quality of communications of the wideband OFDM system in the physical layer.

V. Conclusions

The performance of wideband OFDM system over the coexistence environment is studied to analyze the interference mitigation capability of LDC-UWB. We showed that Mutual collision probability between wideband OFDM systems and LDC-UWB systems could be modeled as the two states Markov collision model. Also, the FER of wideband OFDM systems has been discussed by using computer simulations. We can conclude as that LDC protocol is efficient interference mitigation technique for low data rate UWB radio communications since the FER of wideband OFDM systems are improved with decreasing of the duty-cycle of LDC-UWB. However, this means that the effective low duty cycle imposes the low data rate, essentially.

References

[1] FCC, First Report and Order: In the matter of Revision of Part 15 of the Comission's Rules Regarding Ultra-Wideband Transmission Systems, *FCC 02-48*, April 2002.

[2] Thomas Zasowski, Armin Wittneben, "Performance of UWB Systems using a Temporal Detect-and-Avoid Mechanism", *The International Conference on Ultra-Wideband*, September 2006.

[3] V. S. Somayazulu, J. R. Foerster, R. D. Roberts, "Detect and Avoid (DAA) Mechanisms for UWB Interference Mitigation", *The International Conference on Ultra-Wideband*, September 2006.

[4] Wei Ye, john Heidemann, "Ultra- Low Duty Cycle MAC with Scheduled Channel Polling", *USC/ISI Technical Report ISI-TR-604*, July 2005.

[5] Francesca Cuomo, Cristina Martello, Andrea Baiocchi, Fabrizio Capriotti, "Radio Resource Sharing for Ad Hoc Networking With UWB", *IEEE Jour. on Selec. Areas in Comm.* Vol.20, No.9, December 2002.

[6] William M. Lovelace, J. Keith Townsend, "Chip Discrimination For Near Far Power Ratios In UWB Networks ", *Military Communications Conference 2003 (MILCOM 2003)*, October 2003.

[7] William M. Lovelace, J. Keith Townsend, "Adaptive Rate Control with Chip Discrimination in UWB", *IEEE Conference on Ultra Wideband Systems and Technologies 2003*, November 2003.

[8] Raffaello Tesi, Marian Codreanu, Ian Oppermann, "Interference Effects of UWB Transmission in OFDM Communication Systems", *IEICE Transactions on Fundamentals*, Vol. E89-A, No. 11, pp. 3059-3065.

[9] A. Tomoki, Idnin Paysa, and T. Kobayashi, "Simulation of interference effects from MB-OFDM and DS-UWB to a QPSK digital transmission system", *International Symposium on Ultra Wideband Systems*, January 2003.

[10] Ed Callaway, "Project: IEEE P802.15 Working Group for Wireless Personal Area Networks (WPANs)", *doc.: IEEE 802.15-01/188r1*, May 2001.

[11] K. Fazel, S.Kaiser, "Multi-Carrier and Spread Spectrum Systems", Published by WILEY, 2003, ISBN 0-470-84899-5.

NOVEL IMPLANT POSITION ESTIMATION ALGORITHM USING THE MATCHING METHOD

Kazunari Tai, Hiroki Harada, Ryuji Kohno
Kohno Laboratory, Div. of Phys., Elec and Comp. Eng. Graduate School of Eng., Yokohama National University,
79-5 Tokiwadai, Hodogaya, Yokohama, Kanagawa, 240-8501, Japan.

ABSTRACT

Recently, the use of wireless communications devices in the field of medical implants devices (MIDs) has received great deal of attention due to constant degree of miniaturization of electronic circuits. By means of transmitting vital data such as blood pressure, blood glucose level, heartbeat and photograph of the inside of the esophagus, we can observe the body condition and detect any possible problem in the human body at anytime and anywhere. These devices can help doctors to diagnose and cure diseases.
In order to communicate and to analyze the information delivered by MIDs reliably, information about implant's position is needed. In this paper we propose an algorithm that estimates the position of MIDs using information from cross-section (slice) photographs taken by CT (computed tomography) or MRI (magnetic resonance imaging) systems. Based on simulations, we evaluate which UWB transmission pulse is suited to the proposed method, and we show the effectiveness of a weighting approach on the proposal .

I. INTRODUCTION

Semiconductor technology and circuits technology are quickly evolving so that smaller devices are available and relatively longer-lasting batteries. Furthermore, wireless communication has been developed for nano-size devices. These advances have made possible to implant a network of bio-sensors inside the human body for health monitoring purposes. With bio-sensors inside the human body, we can get the real-time information of activity, diseases, medications and so on. This technology is interesting due to to the potential of improvement in a person's quality of life.

Many MID such as cardiac pacemakers and encapsulated endoscopes are used in a medical setting. In order to control and to communicate with them or with other implanted devices as well as devices outside the body, some information and communication technologies are needed. To reliably communicate or analyze the information of implant devices correctly, accurate information on the implant's position is required. In the literature, many position estimation methods have been reported. However, due to the EM propagation through the body is distorted significantly, such position estimation methods are not effective for the position estimation of MIDs. In this paper we propose a new system to estimate the position of MIDs based on information from cross-section (slice) photographs taken by CT or MRI systems. The estimated wave shapes are calculated using the Finite Difference Time Domain (FDTD) method and the information from cross-section (slice) photographs of the human body. By checking the maximum cross correlation between such estimated wave shapes with the received wave shapes, we can estimate the position of MIDs. We employ Ultra Wideband (UWB) technology, because it achieves high resolution and its devices can be made very small.

This paper is organized as follows: In Section 2, some basic characteristics of EM wave propagation and properties of dielectric materials of the human body tissue are described. In Section 3, the proposed position estimation method is delineated. In Section 4 simulation results are presented. Finally, in Section 5 conclusions are provided.

II. RADIOWAVE PROPAGATION IN A MEDIUM

A. *Propagation of Electromagnetic Waves in Dielectric Materials*

Consider a plane wave, which is traveling in the positive z direction, with polarization in the x direction[1], the electromagnetic fields in a lossy medium are given by

$$E_x = Ak^2 e^{-jkz} = E_0 e^{-jkz}, \quad (1)$$

$$H_y = A(\omega\varepsilon - j\sigma)k e^{-jkz} = H_0 e^{-jkz}, \quad (2)$$

$$E_y = Ez = Hx = Hz = 0, \quad (3)$$

$$k = \sqrt{\omega^2\mu\varepsilon - j\omega\mu\sigma}, \quad (4)$$

where E_0 is the amplitude of the electric field, μ is the permeability, $\varepsilon - j\frac{\sigma}{\omega}$.

The wave impedance is given by

$$\frac{E_x}{H_y} = \frac{E_0}{H_0} = \sqrt{\frac{\omega\mu}{\omega\varepsilon - j\sigma}} = Z_0 . \quad (5)$$

This impedance is complex in a lossy medium and then phase difference occurs. Additionally, the propagation constant is also complex. Figure 1 shows the attenuation of the electric field while traveling in fat tissue. The permittivity of fat is 7.5 and the conductivity is 0.15 S/m at 1.0 GHz. The propagation constant k is generally, separated into real component and imaginary components as [2],

$$k = \beta - j\alpha, \quad (6)$$

$$\alpha = \omega\sqrt{\mu\varepsilon}\sqrt{\frac{1}{2}\left(\sqrt{1+\left(\frac{\sigma}{\omega\varepsilon}\right)^2} - 1\right)}, \quad (7)$$

$$\beta = \omega\sqrt{\mu\varepsilon}\sqrt{\frac{1}{2}\left(\sqrt{1+\left(\frac{\sigma}{\omega\varepsilon}\right)^2} + 1\right)}, \quad (8)$$

where α is the attenuation constant and β is the phase constant.

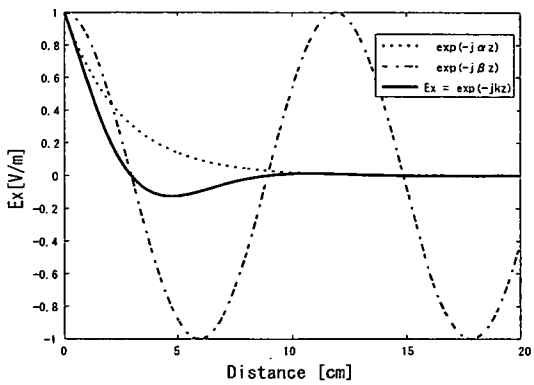

Figure 1: Attenuation of EM wave in a lossy medium.

B. Human Body Tissue

A human body consists of various organs with complex structures. Furthermore, each organ has different characteristics of conductivity and permittivity.

We should consider the frequency band when we try to communicate with implanted devices because of the frequency dependency of σ and ϵ. Generally, if the tissue has a higher percentage of water content, then the relative permittivity and conductivity are high as well. Therefore, the EM wave attenuation will be significant. The measurement of dielectric properties is well known. In [3] the dielectric properties of human body tissues in the frequency range from 10 Hz to 100 GHz are reported.

On the other hand, there are well known dispersions in the dielectric spectrum of biological materials and their expression depends on the main polarization mechanism. The spectrum extends from 10 Hz to 100 GHz and shows four dispersion regions. The complexity of the structure and composition of biological material such that each dispersion region is broadened by multiple contributions, which are described by a Cole-Cole expression [4]. Figure 2 shows the dielectric properties of muscle and fat tissues calculated by the Cole-Cole equation as follows

$$\varepsilon(\omega) = \varepsilon_{\infty} + \sum_{n=1}^{4} \frac{\Delta\varepsilon_n}{1 + (j\omega\tau_n)^{(1-\alpha_n)}} + \frac{\sigma_i}{j\omega\varepsilon_0}. \qquad (9)$$

C. Position estimation methods

As previously mentioned, the human body is a lossy medium and has many tissues that have individual relative permittivity and electrical conductivity.

These features make difficult to employ existing position estimation method for MIDs. For example, the high attenuation and changes in the propagation speed have a bad effect the estimation accuracy of TOA (Time Of Arrival) and RSS (Received Signal Strength) methods. Additionally, the reflection and refraction components also affect the estimate accuracy of AOA

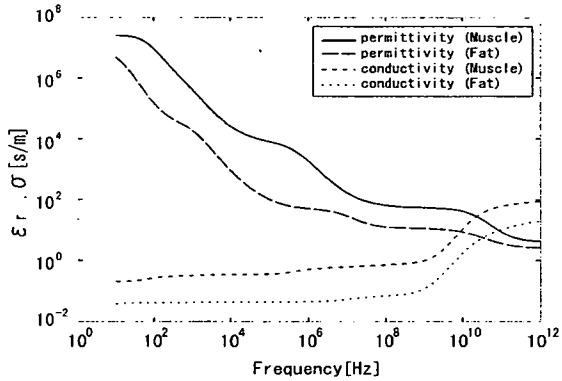

Figure 2: Dielectric parameters of muscle and fat.

(Angle of Arrival) significantly. Therefore, we propose a new method to estimate the position of MIDs.

III. Position Estimation Algorithms

A. The shape of received waves

In the first place, we focus on the shape of received waves. When EM wave propagates through the body it has a characteristic individual shape depending on the location of a target MID. Figure 3 shows an example of received waves (outside the body) transmitted from inside of the body.

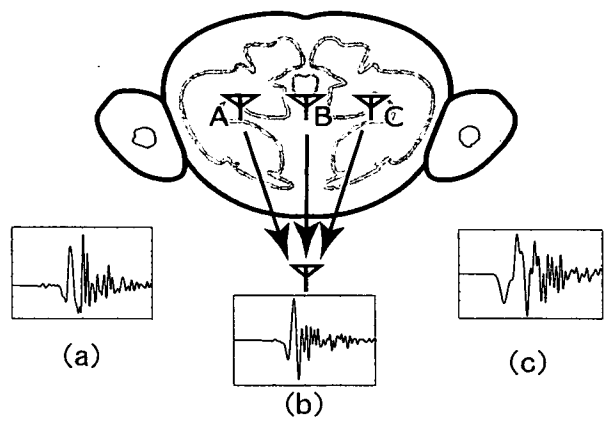

Figure 3: The received waves which are transmitted from different transmitter location.

Accordingly, if we calculate the shape of EM waves, which are transmitted from different positions in the body, we can estimate such a position by matching the observed waveforms with a template waveform that is generated by the FDTD method on a 3D image given by CT or MRI systems.

B. Matching method

1) Calculation of the received wave shapes

First of all, a virtual three dimension human body model is created based on photographs of CT or MRI systems. For each tissue in the model, the different electric parameters are introduced.

We assume that the MID in the 3D model transmits a given waveform to a receiver outside the body. By applying the FDTD method to the 3D virtual model, we calculate the EM waves that are transmitted from different positions in the 3D model. We call this calculated waves as "template waves".

Such transmitting positions are set up on the lattice points of the 3D model. Figure 4 shows the arranging of the lattice points.

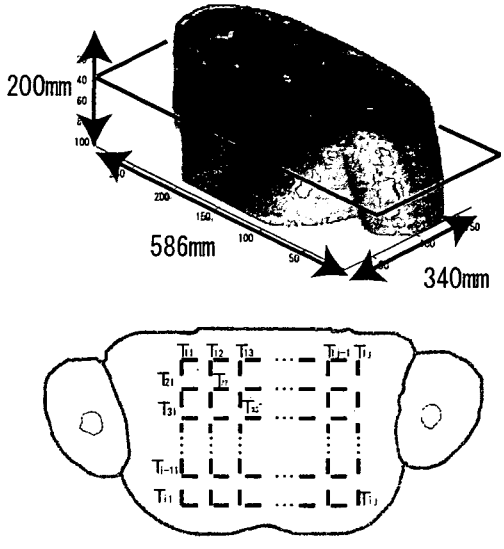

Figure 4: Human body model and example of arranging lattice point.

Figure4 shows a torso cross-section and the lattice points over a 2D plane. When the signal is transmitted from the implant located at each lattice point T_{ij}, the waveform $r'_{kij}(t)$ received by the q^{th} antenna is calculated by FDTD method.

On the other hand, $r_q(t)$ is a received waveform.

2) Matching for position estimation

In order to match $r_q(t)$ with the template waveforms, we calculate the maximum correlation

$$Corr_q(i,j) = \arg\max_{\tau}\left\{\sum_{n=0}^{N} r_q(n) * r'_{qij}(n-\tau)\right\} \quad (10)$$

Finally, the estimated position (i', j') of a given MID is obtained by

$$(i', j') = \arg\max_{(i,j)}\left\{\sum_{q=1}^{K} Corr_q(i,j)\right\} \quad (11)$$

Figure 6 illustrates an example of the proposed matching method.

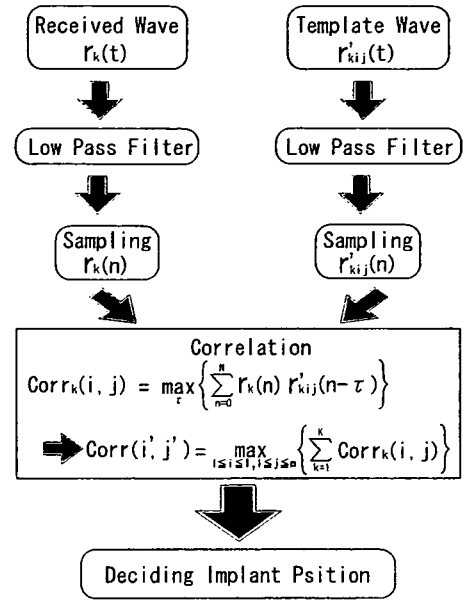

Figure 5: Block diagram illustrating the Matching method process.

IV. Weighted Estimation Method

In order to improve the accuracy of the proposed matching method, we consider weighting each receiving antenna based the received power.

Figure 7 shows a 2D MRI-derived FDTD stomach model that is made from sliced images.

Table 1: Simulation Specification

Used Simulator	XFDTD-Human Body Model (stomach region)[5]
Time step	1.926[ps]
Number of Time Steps	10000[step]
Transmit Waveform	Gaussian Mono Pulse
Used Bandwidth	1.0-3.0[GHz]
Position of Receiving Antennas	(x,y)=(208,73),(403,62), (158,318),(488,303)
Transmission Antenna Interval	1[mm] (x axially)
Analysis Range	(x,y)=(275,180)-(325,180)
Kind of Noise	White Noise

A. Relationship between the accuracy and bandwidth

We analyze the relation between the accuracy of the position estimation and bandwidth of the transmitted waveform.

We calculate the template waveforms in case of the MID is placed from (x=275,y=180) to (x=325,y=180) in the FDTD method. Figure 8 shows the correlation when the position of a MID is placed in (x=300,y=180).

The dotted line in Fig.8 shows the position of the MID (x coordinate). The position of the MID is given by the maximum

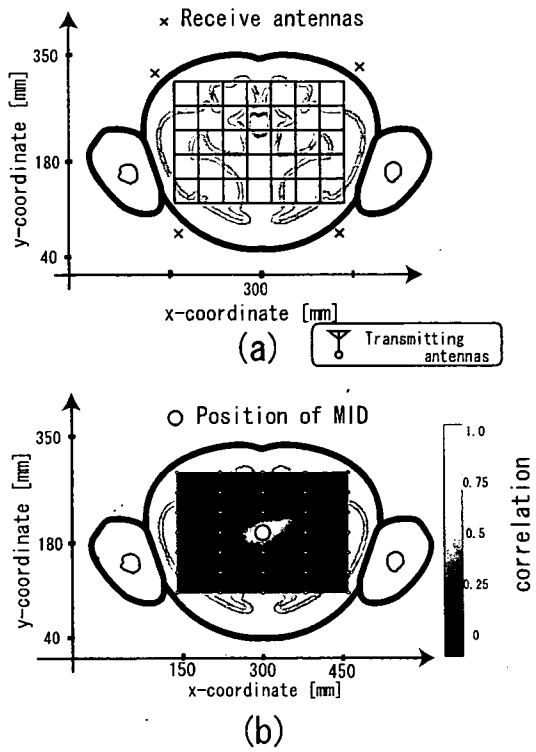

Figure 6: Execution example of Matching method. (a)2=D MRI-derived FDTD stomach model. The transmitting antenna is at the center. The four receiving antennas are at out of the body. (b)Black dot center of the body represent transmitting antenna. The point where the numerical value of Correlation is high is an MID existence position.

correlation. This result shows that the wider the bandwidth of the transmit waveform, the sharper the peak of the correlation function, so a better accuracy of position estimation.

Fig.10 shows RMSE (Root Mean Square Error) against SNR. RMSE is calculated by

$$RMSE = \sqrt{\frac{\sum_{k=1}^{K} l_e(k)^2}{K}} \qquad (12)$$

$l_e(k)$ is the distance error using each antenna. Notice that in spite of the transmitted waveform has high bandwidth (2.5, 3.0 GHz), the RMSE is high. The reason is that high-frequency components are further attenuated and the received power is lower. Based on Figure 8, the waveform with 1.5 GHz bandwidth gives the best result.

B. Weighted generation per antenna

The proposed matching method estimates the position of the MID by using only one antenna. However, we use a number of receiving antennas in order to enhance the accuracy. Furthermore, we weight antennas' output in order to improve the estimation. One of the most important parameters is received power. Such a power changes significantly depending on the distance between transmitter and receiver. If the received power is much lower than noise power, the accuracy becomes

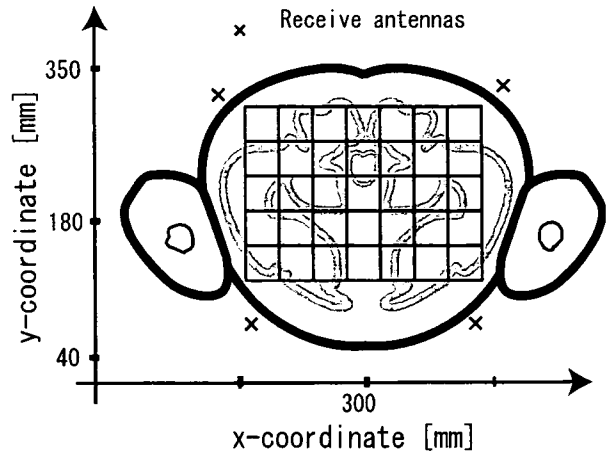

Figure 7: 2=D MRI-derived FDTD stomach model and receiving antenna

poor. In order to generate receiving antenna weights, we analyze the relationship between received power and RMSE, Figure10.

The position is estimated from (x=305,y=180) to (x=345,y=180). In this simulation, a number of antennas is 18. Notice that we increase the number of antennas to observe closer the relationship between SNR and RMSE only. Posteriorly, the number of antennas is set up to 4 again.

All antennas are placed 5 mm from the skin, and are separated 5 cm from each other. The SNR is set up from 5 dB to 25 dB. If SNR is lower than 5 dB, the estimation accuracy decreases and the characteristic of RMSE to the received power is lost. On the other hand, if SNR is higher than 25 dB, the distance error becomes smaller and the characteristic of RMSE to the received power is also lost.

The approximation quadratic curve is calculated as Fig.10.

$$y = 3.4 * 10^3 * x^2 - 1.1 * 10^2 * x + 2.1 \qquad (13)$$

The weighting is done according to y^{-1}.

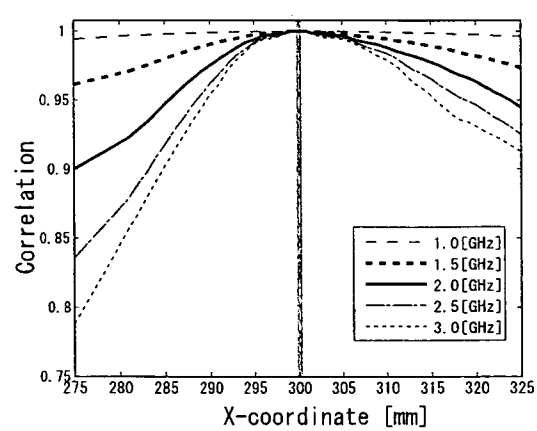

Figure 8: Relation between use band and correlation value. (Not inlude noise)

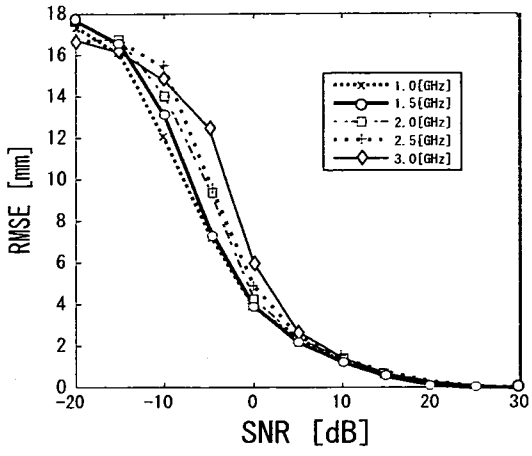

Figure 9: Relation between RMSE and SNR

$$(i', j') = \arg\max_{(i,j)} \left\{ \sum_{q=1}^{K} y^{-1} * Corr_q(i,j) \right\} \qquad (14)$$

Fig.11 shows RMSE when we weight antenna or not. The result shows the improvement of RMSE (SNR=5-25) and also shows the effectiveness of the weighting.

V. Conclusion

In this paper, we proposed and demonstrated Matching method for position estimation of MID. We analyzed the result of position estimation, and showed that 0-1.5GHz frequency band of UWB signal have a beneficial effect on the method. We also proposed the method for whighted generation per antenna. Simulation result showed that proposed method improved the estimation accuracy. In the future, we will simulate the method on 3D model. Furthermore we will consider how the human body motion gives influence to the estimation accuracy.

References

[1] Y. Mushiaki "Antenna and Wave Propagation," Corona Publishing, 2001.

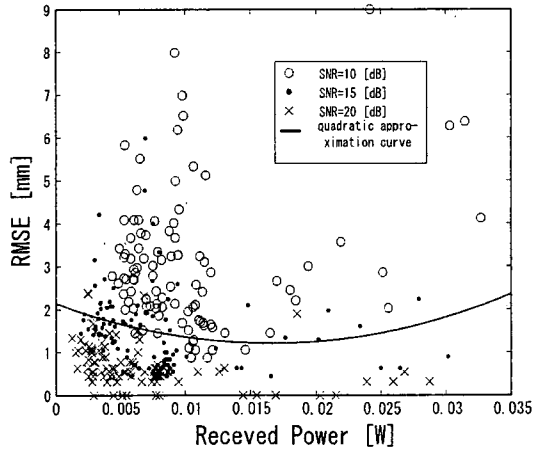

Figure 10: Relation between RMSE and Received Power

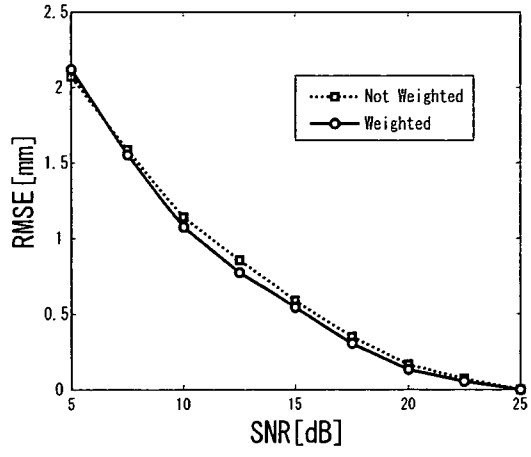

Figure 11: Relation between RMSE and SNR (weighted)

[2] T. Ohmori, "Bio Electromagnetic Engineering and Application ," Fujitec Corporation

[3] C. Gabriel, S. Gabriel, "Compilation of the dielectric properties of body tissues at RF and Microwave Frequencies," http://www.brooks.af.mil/AFRL/HED/hedr/reports/dielectric/home.html

[4] K. S. Cole and R. H. Cole, "Dispersion and absorption in dielectrics : 1. Alternating current characteristics.," *Journal of Chemical Physics*, Apr. 1941.

[5] Remcom. Inc,. http://remcom.com

NOVEL MAC PROTOCOLS CONSIDERING THERMAL INFLUENCE IN AN IMPLANTED BODY AREA NETWORK

Shun Nagamine, Hiroki Harada, Ryuji Kohno
Division of Physics, Electrical and Computer Engineering, Yokohama National University
79-5 Tokiwadai, Hodogaya, Yokohama, 240-8501, Japan
Tel: +81-45-339-4116, Fax: +81-45-338-1176
E-mail:shun,hhiroki@kohnolab.dnj.ynu.ac.jp, kohno@ynu.ac.jp

ABSTRACT

Recently, the use of wireless communications devices in the field of medical implants has received a great deal of attention due to the increasing degree of miniaturization of electronic circuits. By means of transmitting vital data, we can observe the body's condition and detect any possible problem in the human body at anytime. However, in the face of vulnerability of cells to radiation absorbtion, quantified in terms of temperature rise, it is expected to raise concern of the electromagnetic wave exposure when nodes communicate. Power-efficient information gathering is preferable than long term continuous duty for nodes implanted in a human body. So, we assume that a sensor network inside the body takes a clustering form and switching leadership between a few of nodes in order to control their thermal influence. In this case, leader's reception mode takes a long time, since several nodes attempt to communicate at once. Then, how to receive information efficiently is significant issue for controlling the thermal influence. In this paper, we propose a protocol that controls the thermal influence by considering media access control (MAC). Finally, we show that the proposed protocol can control the thermal influence better than existing MAC protocols.

I. INTRODUCTION

With the increased sophistication of semiconductor technology, smaller wireless communication devices have been developed. Now a days these devices are used in medical implanted applications. In the near future, wireless communication devices with a sensor function can be implanted (node) in human body, forming a sensor network. Each node can monitor health data such as blood pressure, blood glucose level and pulsation, and to transmit those to a medical server. However, it is difficult to apply current sensor network technology directly to the human body, because of the vulnerability of cells to the thermal influence caused by electromagnetic wave exposure.

A power-efficient information gathering structure is necessary because it is preferable that long term continuous duty for nodes implanted in a human body[1]. The received power depends on the transmission distance, so it is advisable to take a clustering form for controlling power consumption.

In a clustering form, neighbor nodes form a cluster, where a full function device (FFD) is the cluster leader that gathers health data from another nodes that belong to the cluster. The FFD interfaces with a medical server outside the body. Therefore, in this paper we use the clustering form as a system model.

In this case, the leader consumes more power than the other nodes. So, it offers a higher rise of thermal influence.

Consequently, we can choose which node is the leader, switch leadership to another node in order to disperse the thermal influence. For temperature rise caused by thermal influence, we employ an approximation of the Pennes' biologic thermal transport equation that is often used as the computation approach of heat propagation in a human body caused by electromagnetic waves.

In active mode, the leader collects information from all the non-leader nodes (reception mode) and posteriorly the leader transmits the information to a receiver outside the body (transmission mode). Notice that reception mode takes a longer time since the information of several nodes must be collected. Thus, this longer time increases the risk of temperature rise (thermal influence). In this paper, we propose a method for controlling the thermal influence by considering MAC.

In Section II, we describe the system model. We discuss the calculation of SAR and temperature increment in Section III. We compare a collision avoidance system with a non-collision avoidance system and propose a MAC protocol for controlling the thermal influence in Section IV. In Section V, we evaluate the proposed protocol and compare its results with existing MACs through simulation. Finally, conclusions are given and we describe future works in Section VI.

II. SYSTEM MODEL

A. *Cluster-based Networking and Switching of Cluster Leader*

Since implanted biosensors must operate with very limited power, energy efficiency is an important aspect of design. Prior research shows that a cluster-based communication protocol (CB) is more energy efficient than a tree-based approach[2]. CB is based on the idea that energy consumption can be reduced by having particular nodes performing long range communication with a receiver outside the body. These nodes are called cluster leaders. The FFD is equipped with more complex circuits. So, all the non-leader nodes are denominated as reduced function devices (RFD) that contain simple sensors, a processor, and a transceiver. We assume that a cluster consists of a couple of FFDs and a number of RFDs, see Fig. 1.

We propose switching leadership between a couple of FFDs to disperse the thermal influence.

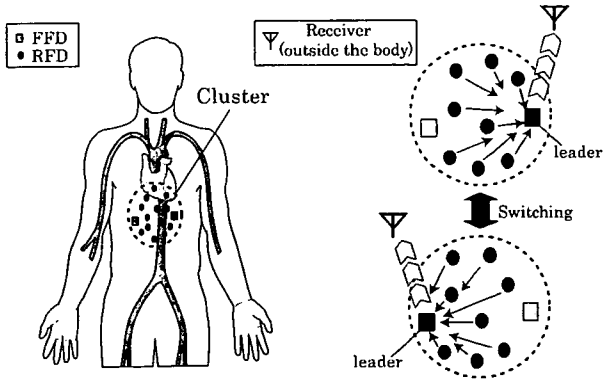

Figure 1: System Model:A cluster of implanted sensoers

B. *Thermal Influence*

Essentially, the temperature surrounding the node can be measured by using a temperature sensor inside the the FFD or RFD circuitry, but this will raise the cost and increase the complexity of the sensor circuit and the strain for the patient when it is implanted. So, in this application we assume that nodes cannot measure the surrounding temperature. Consequently, we compute the expected temperature by the FDTD method preliminarily, and we compare the proposed MAC algorithm with existing MACs based on this result.

III. Temperature Computation

We compute the temperature of leader, because RFDs consume much less power than the leader.

For safety reasons, the level of radiation being absorbed by the human body needs to be limited. The specific absorption rate (SAR) is the rate at which radiation energy is absorbed by tissues per unit weight.

The relationship between radiation and SAR is given by

$$SAR = \frac{\sigma|E|}{\rho} \text{ (W/Kg)}, \tag{1}$$

where σ is the electrical conductivity of the tissue, E is the RMS induced electric field, and ρ is the density of tissue.

Many organizations set strict standards for peak spatial-average SAR, but these standards are based on exposure from sources outside the body. In our application, we assume that RF powering source is implanted depth inside the body. Consequently, we consider the thermal influence by using the a modification of the Pennes' biologic thermal transport equation[3] given by

$$\rho C_p \frac{dT}{dt} = \kappa \nabla^2 T - \rho\rho_b C_b F(T - T_b) + \rho SAR, \tag{2}$$

where $\rho(\rho_b)$ is the tissue (blood) density, $C(C_b)$ is the specific heat of the tissue (blood), κ is thermal conductivity of the tissue, $T(T_b)$ is the temperature of the tissue (blood), F is flow rate of blood.

The first term of right-hand side in Equation 2 indicates the thermal propagation by surrounding cells. The second term indicates the cooling effect by flow of blood and the third term indicates the heat generated due to radiation. However, we apply the equation under the following conditions.

- We do not consider the effect of heat exchange with the air as the nodes are inside the body.
- The temperature in the boundary of calculating area is 37°C.
- We consider even capillary vessel as blood vessel.

We calculate the SAR by using the three-dimensional field analytic simulator XFDTD[4]. FDTD is an electromagnetic modeling technique that discretizes the differential form of time and space.

Fig.2 illustrates a distribution chart of the SAR in the clustering arreagment with a FFD and ten RFD nodes, which are randomly-located. In this paper we do not discuss physical layer, so we ignor attenuation of a signal, bit error rate, and so on. Additionally, we configure the distance between the leader and the receiver outside the body is much longer than the one between the leader and each RFD node. The power consumption of the cluster leader in active mode is 5 mW, and 0.5 mW for the RFD nodes[5]. The RF waves have sinusoidal variation with frequency 2.45 GHz. The size of the calculating area is 100 mm × 100 mm. The size of a cell is 1 mm × 1 mm. The surrounding medium of a leader is assumed to be homogenous muscle.

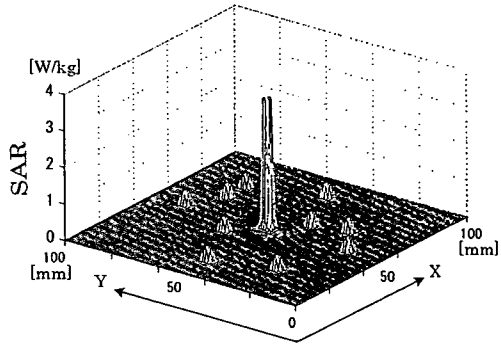

Figure 2: Distribution chart of the SAR

As shown in Fig.2, the distribution of the SAR is very small (except in the FFD node) so we can ignore it. Equation 2 indicates that the temperature increment is local if the distribution of the SAR is local. For that reason, we consider the temporal character of temperature increment in the leader position, only.

In addition, each FFD node is placed as far as possible from each other, so we assume that the cause of thermal effect is produced by a single FFD node.

When using Equation 2, the entire space is discretized into small cells that are marked with a pair of coordinates (i, j)[6]. So, we derive a new bioheat difference equation from 2. After some mathematical manipulations is given by

$$T_{i,j}^{n+1} = \left(1 - \frac{2\kappa\Delta t}{\rho C_p}\left(\frac{1}{\Delta x^2} + \frac{1}{\Delta y^2}\right) - \frac{\rho_b C_b F \Delta t}{C_p}\right) T_{i,j}^{n} + \frac{\kappa\Delta t}{\rho C_p}\left(\frac{T_{i+1,j}^{n} + T_{i-1,j}^{n}}{\Delta x^2} + \frac{T_{i,j+1}^{n} + T_{i,j-1}^{n}}{\Delta y^2}\right) + \frac{\Delta t}{C_p}(\rho_b C_b F T_b + SAR) \quad (3)$$

where $T_{i,j}^{n+1}$ is the temperature of the cell point (i, j) at time $n + 1$, Δt is discretized time step, Δx and $\Delta y$is discretized space step. From Equation 3, we can find the temperature of the cell point (i, j) at time $n + 1$ from the temperature of cell at point (i, j), time n and the temperature of surrounding cell at points((i+1,j),(i-1,j),(i,j+1) and(i,j-1)) at time n.

Figure 3 shows the temporal character of temperature increment when there is no leader rotation. So, the tissue surrounding the leader is heated continuously. In this simulation, we assume that the medium in which the leader exists is muscle because it comes in a larger proportion relative to other tissues or organs. Furthermore, muscle is more susceptible to thermal influence than other tissues or organs.

Simulation parameters for obtaining Figure 3 are shown in Table 1, and the value of SAR is obtained from Equation 3 for the clustering arraignment illustrated in Figure 2.

Table 1: Parameters of muscle and blood.

parameter	value
$C_p(C_b)$	3.5e+3(3.9e+3)$[J/kgK]$
$\rho(\rho_b)$	1.070e+3(0.94e+3)$[kg/m^3]$
κ	0.59$[W/mK]$
F	0.45e-6$[m^3/kgs]$

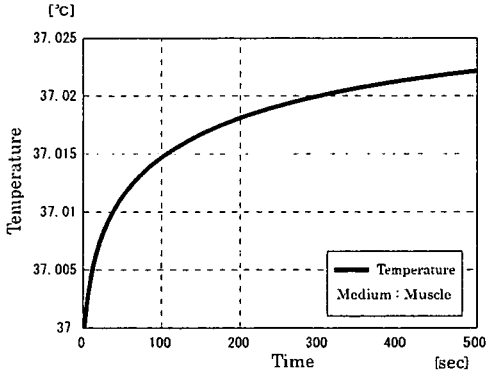

Figure 3: Temporal character of temperature increment.

IV. MEDIA ACCESS CONTROL

As previously noted, the leader receives the information from a number of RFD nodes in reception mode. So, it is expected that the processing time in that mode changes significantly depending on the number of RFD nodes and media access control. Therefore, we propose a new MAC protocol, which is effective at collecting the information from each node to the leader in order to control the thermal influence.

The IEEE 802.15.4 standard for Low Rate-Wireless Personal Area Network (LR-WPAN), applies the frequency bands 868 MHz, 915 MHz, 2.45 GHz, and date rate 20 kbps, 40 kbps, 250 kbps, respectively. We based the proposed MAC protocol on such standard. On the other hand, the implanted nodes inside the body are expected to be low-cost and simple, where the amount of information is relatively small. For these reasons, we assume that the proposal is in line of IEEE 802.15.4 (2.45 GHz/250 kbps)[7].

A. *Existing Protocols*

1) *CSMA/CA protocol*

In the CSMA/CA (Carrier Sense Multiple Access with Collision Avoidance) protocol, nodes send data frames using the carrier-sense autonomously in order to share a channel with other nodes. In the carrier-sense, a node decides whether or not it sends data frames after sensing usage of the channel to avoid collision of frames with other nodes. If the channel is assumed to be busy, the frames are postponed temporally. If not, a node assumes the channel to be idle and then begins to send frames. The algorithm of carrier-sense is briefly shown in Fig.4.

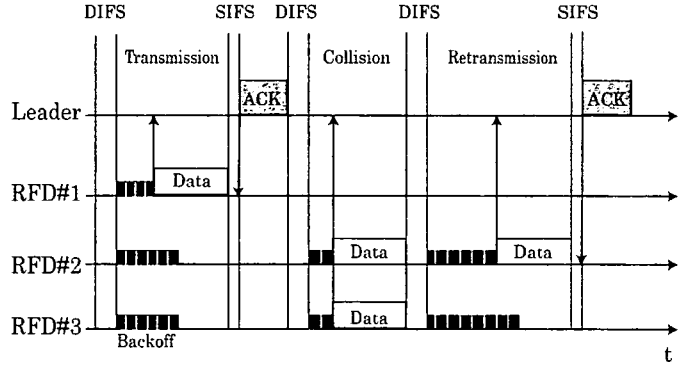

Figure 4: CSMA/CA algorithm

In particular, a node waits for DIFS (DCF Inter Frame Space) time when the state of the channel usage changes from busy to idle in its carrier-sense. After that, a backoff that is a carrier-sense for a random time is started and the node can begin to communicate if it recognizes that the state is idle continuously. In the backoff, collisions are avoided by the carrier-sense for a random time. The backoff time is defined as:

$$Backoff time = Random \times Slot time, \quad (4)$$

where *Random* is a random integer number that is generated from a uniform distribution in [0,CW]. CW is also an integer number between CWmin and CWmax. In order to decrease a probability of collision CW increases its range as follows:

$$CW = (CWmin + 1) \times 2^n - 1, \quad (5)$$

where n is the number of retransmission.